Sky Tessellation Patterns for Field Placement for the All-Sky H I Survey WALLABY

Bradley E. Warren

International Centre for Radio Astronomy Research, University of Western Australia, M468, 35 Stirling Highway, Crawley WA 6009, Australia; bradley.warren@icrar.org

Version 0.9, May 6, 2011

ABSTRACT

We present a preliminary investigation of possible field placement strategies for the upcoming all-sky H I survey WALLABY, proposed for the Australian Square Kilometre Array Pathfinder. We examine two methods for tessellation of a sphere, Declination Bands and HEALPix, to see if they can be used to generate a field placement pattern for the survey that can cover the sky south of $\delta = +30^\circ$ in an efficient manner. We find that Declination Bands is an efficient and adaptable method of field placement, and that we can ensure that there are no gaps occur between fields using this method. It has the minor disadvantage of having large overlap areas between fields close to the poles, though we can mitigate this some what by using a different strategy in this region. HEALPix on the other hand does not appear to be an appropriate method of field placement, being much less efficient, inflexible, and not covering all regions of the sky without significant adjustments or a higher tiling density. HEALPix would instead be better used at the later processing stages of the survey for producing cubes for all-sky analysis, a purpose much closer to that which it was originally designed for.

1. Introduction

The Widefield ASKAP L-band Legacy All-sky Blind surveY (WALLABY[1]) is one of the major Survey Science Projects currently proposed for the Australian Square Kilometre Array Pathfinder (ASKAP). It is intended as the next generation all-sky extragalactic blind H I line survey, going significantly deeper, at higher spatial resolutions, and to higher redshift than

[1]Original proposal abstract at http://www.atnf.csiro.au/research/WALLABY/proposal.html

similar previous H I surveys like the H I Parkes All-Sky Survey (HIPASS, Barnes et al. 2001). WALLABY aims to detect 21 cm line emission in up to 500,000 galaxies out to $z \sim 0.26$ over the 3π steradians of the sky south of $\delta = +30°$ (the remaining northern quarter of the sky will potentially be covered by the proposed Westerbork Northern Sky H I Survey, WNSHS).

ASKAP is an aperture synthesis array currently under construction at the Murchison Radio Observatory in mid west Western Australia, and when completed will consist of 36 antennas 12 m in diameter with a maximum baseline of 6 km. The full array will have a spatial resolution of $\sim 10''$ around the rest frequency of H I, or $\sim 30''$ if only the 30 antennas within the inner 2 km are used, with a velocity resolution of $\sim 4\ km\,s^{-1}$. Each ASKAP antenna will be equipped with a phase array feed Focal Plane Array (FPA), with a field-of-view (FoV) of ~ 30 deg^2, allowing faster survey speeds of large areas of the sky. WALLABY and other all-sky ASKAP surveys will require an efficient method of tiling the sky with this large field, the original proposal stating that this should be done "in about 1200 fields, tiled with minimal overlap."

This study is intended as an initial exploration of possible field placement strategies for WALLABY, and by extension other ASKAP all-sky surveys. It is not meant to define the final field placements or even the final method for choosing those placements. In this memo we will compare two tessellation methods, Declination Bands and HEALPix, to see if they are capable of defining a field placement pattern appropriate for the survey.

The primary criteria for distinguishing the methods will be efficiency, which we define as the 3π steradians target area for the survey divided by the total area covered. So the main aim of each method is to keep the overlap between neighbouring fields to a minimum. While there is nothing wrong with having overlap (and therefore regions with deeper observations) between fields, in a survey that will take a year of observing time to complete having an excessive number of extra fields will increase the time required to complete the survey significantly (100 extra fields would be a little over a month of extra observing time on the sky, plus overheads).

2. Simplifications for this Initial Study

At the time of this memo (mid 2011) ASKAP is still under construction, the focal-plane arrays are yet to be tested, and the beam positions and dithering pattern to be used have not been finalised. Therefore the exact details of the FoV (sensitivity variation, shape, the drop-off at the edge of the field, required overlap, etc.) are not determined at this stage. Indeed, they may not be well defined until close to the start of the survey observations.

So for this initial study we adopt a simple model of the ASKAP FoV until more accurate representations become available.

The approximation to the ASKAP field we are using is a simple square of $5.^{\circ}2 \times 5.^{\circ}2$ ($\sim$ 27.02 sq. deg.). The field is effectively treated as a 'black box' when it comes to sensitivity, the region within the field having the target sensitivity with a sharp drop to zero at the field edges (similar to as if we were using a large optical CCD array to cover the sky). Both the field shape and the sensitivity are highly idealised, and likely only to be an rough approximation to the usable area of the final field. The shape of the real FoV and sensitivity variation will depend on the beam configuration of the FPA chosen and the dithering pattern chosen. It will only be approximately square (if that shape is to be used), the drop-off at the field edges will depend on the beams that compose the field and their configuration, and producing even sensitivity across the field may prove expensive in terms of observing time, overhead, and computation (the Survey Science Teams have requested sensitivity variations across the field of less than 10%).

This memo is not intended to explore methods of producing flat sensitivity over a field, or producing square FoVs. Nor are we implying that the FoV will be a flat square, or that this particular field shape be the final configuration of the field. Our simple field approximation should be treated as the minimum useful area of the ASKAP FoV that can be used as a regular griddable shape, which can be used to ensure there are no regions between fields where the sensitivity is below the survey target and account for any overlap that might be needed. Therefore, any sky tessellation method we choose should be flexible enough to deal with changes in the lead up to the commencement of observations. A later memo in this series will look into how the tessellation performs with a more realistic model of the ASKAP FoV.

Calculation of the sky tiling patterns was carried out in SM primarily for plotting purposes, but can be implemented in any programming or plotting language. Calculations for Declination Bands tiling require only simple spherical coordinate transformations, while equations for HEALPix are outlined in Górski et al. (2005) and are likewise relatively simple.

3. Declination Bands

The first method we have tested in this initial study is a simple configuration we will refer to as Declination Bands (or δ-Bands). It is similar to the pattern used for HIPASS (Barnes et al. 2001; Staveley-Smith 1997), and other all-sky surveys such as 2MASS (Skrutskie et al. 2006), though in both of these cases the 'fields' are composed of scans along the declination

axis (in the case of HIPASS a field consists of a series of these scans covering a $8^\circ \times 8^\circ$ region). Fields are placed uniformly around rows of the same declination, all orientated with one axis of the field in the declination direction (i.e. no rotation). Rows are separated by slightly less than the height of one field (see following section), and the number of fields per row is determined by the minimum number of fields required to cover the δ band without gaps.

3.1. Tessellation Pattern

The calculation of the location of each band was started from the northern edge of the target area ($\delta = +30^\circ$ currently) in order to minimise the overlap of fields into the region north of this boundary. While this creates extra overlap at the South Celestial Pole (SCP), the area involved is relatively small (less than one field) compared to the potential extra area needed if we started at the pole (up to the area of a band at that declination). From this stating point the height of the northern-most row and the number of fields in it is calculated, before moving to the next row south, and continuing until the SCP is reached.

Fig. 1 shows a close-up view of a field towards the SCP on an orthographic projection as an example of how the field positions were calculated. The simplified ASKAP field is the square marked in blue, with the black background lines showing the δ-Bands field pattern (all of which follow lines of either constant RA or Dec). The points marked in red show the positions in each field that define the separations between fields for bands in the Southern Hemisphere (for the Northern Hemisphere this is simply flipped vertically). The field shown is centred at $\delta = -80^\circ 51' 28''$, chosen to emphasise the various distortions at declinations towards the poles. The field separations are calculated as follows.

The number of fields in each band was determined from the minimum number of fields needed to completely circle the sky at the declination closest to the equator within that band (i.e. the largest declination ring on the Celestial Sphere within the band). This declination, which we will refer to as δ_0, will be the centre of the northern edge of every field for bands entirely in the Southern Hemisphere (point 0 in fig. 1), the centre of the southern edge of every field for bands entirely in the Northern Hemisphere, and $\delta_0 = 0^\circ$ for any band that crosses the celestial equator. The maximum separation allowed between neighbouring fields in a rows without gaps is then set from the RA difference between the positions where δ_0 crosses the eastern and western edges of the field (between points 1 and 3 in fig. 1). This is given by:

$$\Delta\alpha_{1,3} = 2 \arcsin\left(\frac{\sin(w_x/2)}{\cos\delta_0}\right) \qquad [radians], \tag{1}$$

where $\Delta\alpha_{1,3}$ is the field separation (RA difference from point 1 to point 3), and w_x is the

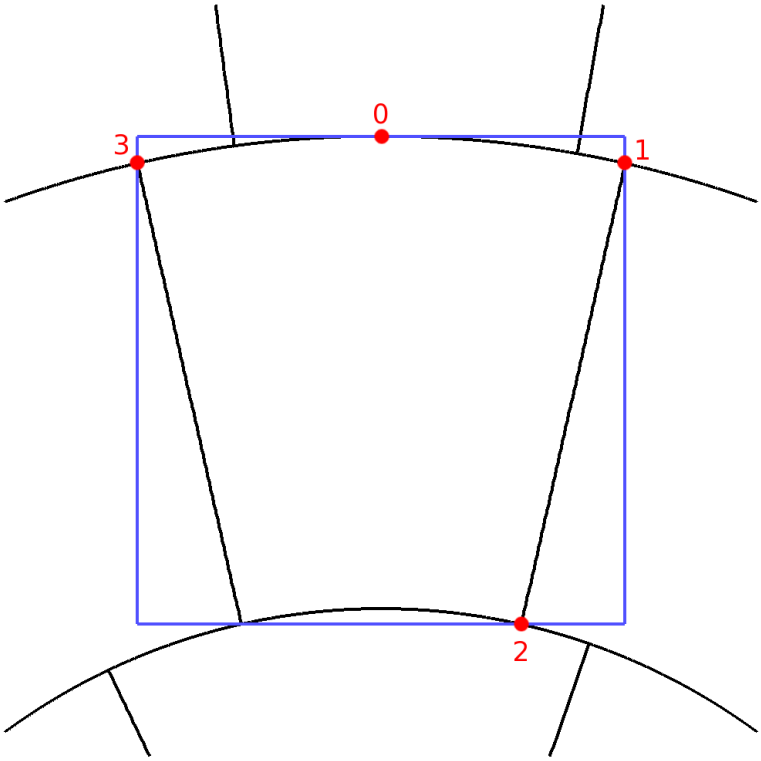

Fig. 1.— Close-up view of one Declination Band field in the Southern sky ($\delta_{centre} = -80°51'28''$) showing the positions in the field that determine the separation between fields. The black lines show the grid of the Declination Band field placements, and follow lines of constant declination (curved lines running approximately horizontal, marking the separation between rows of fields) or lines of constant right ascension (short straight nearly vertical lines, separating fields within a row). The blue square is the simplified approximation to the ASKAP field of view used for the calculations in this work (a $5.^{\circ}2 \times 5.^{\circ}2$ square). The red numbered points mark the positions that define the field separations (see text). The projection is orthographic, along the centre line of the projection North is up, East is to the left.

width of an ASKAP field. The number of fields is then simply $2\pi/\Delta\alpha_{1,3}$ rounded up to the nearest integer. As there is only a small chance of a row requiring an exact integer number of fields, there will almost always be a small area of wrap (less than one field) between the first and last field. So instead of using $\Delta\alpha_{1,3}$ for the separation between fields they were spread evenly around the band, spreading out the wrap overlap.

The separation between rows varies slightly with declination as lines of constant declination are not geodesics, and in all practical cases the separation is slightly less than the height of an ASKAP field. The separation of each δ band was calculated along a line of

constant RA (which are geodesics) starting from one of the points where δ_0 crosses field edge (point 1 in fig. 1), and going down to where the same RA line crosses the base of the field (point 2 in fig. 1). In the Southern Hemisphere the declination at the base of that band (and the start of the next band), which we will refer to as δ_2, is given by:

$$\delta_2 = \arctan\left(\cos\left(\arcsin\left(\frac{\sin(w_x/2)}{\cos\delta_0}\right)\right)\tan(\delta_0 - w_y)\right) \qquad [radians], \tag{2}$$

where w_x and w_y are the width and height of an ASKAP field, respectively ($w_x = w_y$ for our square simplified field).

In the Northern Hemisphere the situation is reversed, starting at the northern edge and heading towards the CE, so we know δ_2 initially but not δ_0 for each band. We have to use an estimate of δ_0 ($\delta_2 - w_y$), use it to calculate a better estimate of δ_0, and iterate until satisfied (in this implementation there were only three iterations, a more robust criteria may be set in future, though the errors are already sub-milliarcsecond for the region we cover). Each new estimate is given by:

$$\delta_0 = \arctan\left(\frac{\tan\delta_2}{\cos\left(\arcsin\left(\frac{\sin(w_x/2)}{\cos\delta_{0,est}}\right)\right)}\right) - w_y \qquad [radians], \tag{3}$$

where $\delta_{0,est}$ is the previous estimate of δ_0.

The SCP is treated slightly differently. If the area of the row containing the SCP will fit into the ASKAP field ($\delta_0 \leq (w_y/2 - 90°)$ and $\delta_0 \leq (w_x/2 - 90°)$) then a single field centred at $\alpha = 0°$, $\delta = -90°$ is used. If the area does not fit into the field then it is treated as a regular band. In the case that is calculated for this memo the former situation of a single polar field applies.

3.2. Results

Using the δ-Bands tessellation pattern described above, with the northern edge of the survey set to $\delta = +30°$, and ASKAP field dimensions of $w_x = w_y = 5.^\circ2$, we can cover the entire WALLABY target area with 1201 ASKAP fields. These fields cover a total area of sky of 32452.78 sq. deg., only 1513.06 sq. deg. more than the 3π steradians target area of the survey. This makes the Declination Bands technique 95.34% efficient (where we define efficiency as the target area divided by the area covered).

Table 1 gives the details for each individual row of the δ-Bands tessellation pattern, including declination centres, right ascension separations, efficiency, and overlap area. The

Table 1. Properties of each row calculated for the Declination Bands tessellation pattern.

Band	δ_{centre} (°)	Fields	$\Delta\alpha_{1,3}$ (°)	$\Delta\alpha_{even}$ (°)	Efficiency (%)	Total Overlap (sq. deg.)	Wrap Overlap (sq. deg.)
(1)	(2)	(3)	(4)	(5)	(6)	(7)	(8)
1	+27.431041	63	5.730133	5.714286	96.9997	51.075047	4.709509
2	+22.256414	66	5.522014	5.454545	96.6487	59.767735	21.792533
3	+17.076364	68	5.370632	5.294118	96.9869	55.365125	26.178508
4	+11.891037	69	5.269174	5.217391	97.9407	38.394864	18.326601
5	+6.700492	70	5.213354	5.142857	98.0816	36.286197	25.578666
6	+1.504703	70	5.200000	5.142857	98.7995	22.708013	20.788648
7	-3.694169	70	5.200949	5.142857	98.6078	26.334018	21.129894
8	-8.887739	69	5.231492	5.217391	98.9432	19.703579	5.027151
9	-14.076088	68	5.306155	5.294118	98.4699	28.114859	4.169859
10	-19.259204	67	5.427990	5.373134	97.1703	51.230754	18.299724
11	-24.436993	65	5.602273	5.538462	96.4945	61.571144	20.008972
12	-29.609268	62	5.837099	5.806452	96.5046	58.558887	8.798807
13	-34.775740	59	6.144367	6.101695	95.7019	68.523538	11.075186
14	-39.935995	56	6.541426	6.428571	94.0086	90.662563	26.106875
15	-45.089469	52	7.053823	6.923077	93.0934	97.045538	26.045194
16	-50.235393	47	7.720086	7.659574	93.1764	86.660745	9.957543
17	-55.372730	42	8.600474	8.571429	92.4736	85.417187	3.834087
18	-60.500063	37	9.794077	9.729730	90.7881	92.099948	6.570833
19	-65.615431	32	11.475279	11.250000	87.8127	105.381817	16.978777
20	-70.716082	26	13.981090	13.846154	86.2255	96.774035	6.782819
21	-75.798146	20	18.057642	18.000000	83.0465	91.621622	1.725689
22	-80.856609	14	25.756771	25.714286	76.7691	87.882534	0.624209
23	-85.889285	8	45.684354	45.000000	61.4673	83.296695	3.239355
24	-90.000000	1	—	—	31.2375	18.580626	—

Note. — Col. (1): Band (or row), starting from the Northern edge of the survey. Col. (2): Declination of the field centre for all fields in the band. Col. (3): Number of fields per band. Col. (4): The RA difference between points 1 and 3 in fig. 1, representing the maximum separation allowed between fields in a band. Col. (5): The RA separation between fields if the fields are spread evenly around the band. Col. (6): Efficiency of the tessellation within the band expressed as a percentage (target area of the band divided by the area covered by the fields in that band). Col. (7): The total overlap area between fields in a band, the area observed in excess of that required for the band (the area covered by the fields in that band minus the area of the band). Col. (8): The overlap area due to the 'wrap' region between the first and last field in a band (in practice this is spread over all fields in the row).

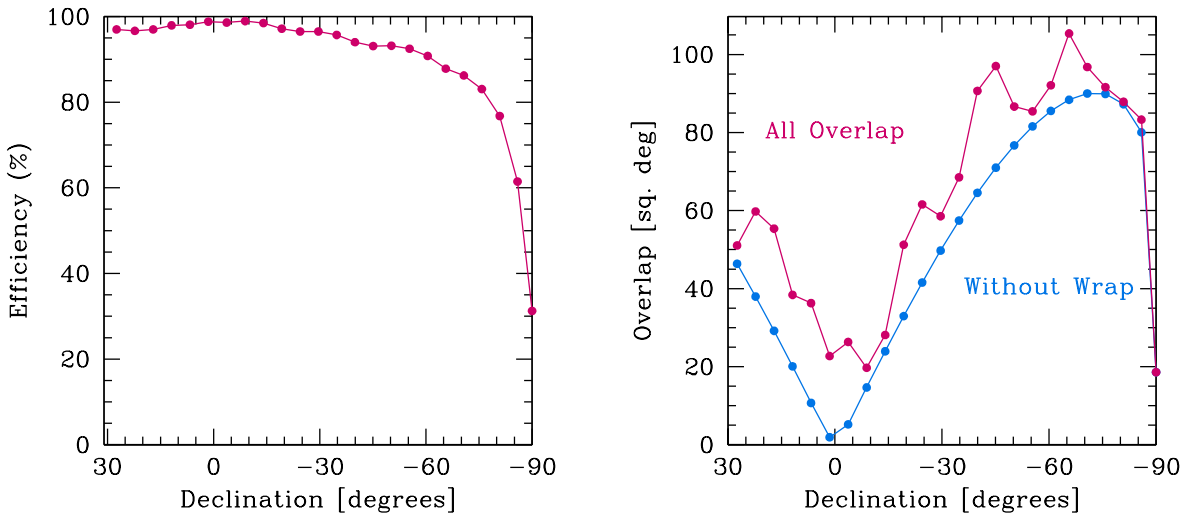

Fig. 2.— (Left panel) Efficiency (target band area divided by the area covered by the fields) vs Declination for the Declination Bands tessellation strategy, showing the rapid decline in efficiency at the South Celestial Pole. (Right panel) Overlap vs Declination for the Declination Bands tessellation strategy. The magenta line shows the all overlap between fields, while the blue line excludes the 'wrap' overlap between the first and last field in a band.

method needs 24 declination bands from the northern boundary to the SCP, with field numbers per band varying from 70 for three equatorial bands to just a single field covering the SCP. The efficiency is highest for the bands closest to the equator, with band 6, the band that crosses the equator, having the highest efficiency of 98.80%. Efficiency declines moving away from the equator to the poles, but over most of the survey area it remains very high. Fields centred in the range $+30° > \delta > -30°$ (over two-thirds of the survey target area) are over 96% efficient, and even band 18 which is centred at $\delta \sim -60.^{\circ}5$ is slightly over 90% efficient. Towards the SCP the efficiency drops rapidly, with the second last band only at ∼61.5%. The last band is a special case as it is only a single field covering the small region at the SCP not covered by previous full rows, and as such is only ∼31.2% efficient. The left panel of fig. 2 shows a plot of Efficiency vs Declination for the δ-Bands method, clearly showing the decline in efficiency in the region surrounding the SCP.

While the fields around the SCP are much less efficient than those at higher declinations, the actual number of fields involved is small compared to higher declinations, and thus the overlap area between fields for these bands is not especially high. The SCP band, while very inefficient, has the lowest overlap area of any band as it consists of only one field. The right

panel of fig. 2 shows overlap (area covered by the field in a band minus the band target area, magenta line) as a function of declination. There are four main sources of overlap; overlap between neighbouring fields in a band, which grows towards the poles as fields become more wedge-shaped; overlap between bands, which also grows moving away from the equator (but dropping to zero at the SCP due to other sources of overlap dominating); the field at the SCP; and the 'wrap' overlap between the first and last field in a row (in practice this would be spread over the whole band). This latter source varies depending on the fraction of a field left over after fitting an whole number of fields around the band, so to see the other effects that vary more smoothly with declination we subtracted this wrap overlap from the total overlap to get the blue line in the right panel of fig. 2. The peak of the overlap from all sources except wrap is around band 20 ($\delta \sim -70.^{\circ}7$), while it is the previous band if wrap is included. The wrap is the dominant form of overlap for the equatorial fields.

Fig. 3 shows a view of the Declination Bands tessellation pattern calculated here projected onto the surface of a sphere. The projection is orthographic and displayed as if viewed from outside the celestial sphere, and the projection centre is located at $\alpha = 43.55^{\circ}$ $\delta = -29.61^{\circ}$ (the centre of a field in band 12). North is up, east is to the left, with the equator and $\alpha = 0^{\circ}$ marked with the red dashed lines. The black lines show the boundaries of the fields, from the northern boundary towards the top of the image to the SCP field (the small circular field near the bottom). Fig. 4 shows close-up views of two region of the sky surrounding individual field, one field from band 20 ($\delta = -70.72^{\circ}$) and the SCP field (we are showing fields at high latitudes as those closer to the equator have minimal overlap). In both images the approximation to the ASKAP FoV for the central field (blue box) and the surrounding fields (red boxes) are overlaid onto the δ-Bands tessellation pattern (black lines). They show the overlap between fields, especially for those fields around the pole where several sizeable patches are covered by up to four overlapping fields.

Overall Declination bands is an efficient technique for field placement in WALLABY. It is also flexible, with the field parameters adjustable to account for any extra overlap that may be required, and some flexibility in field positioning (though depending on the desired changes this may require an increase in the fields needed). The organisation of fields into bands of declination also allows for an easy field indexing scheme (starting either at the pole or the northern limit). The only minor drawback to this method is the clustering of overlap regions towards the SCP. This leads to some small patches of sky covered by up to four times the observing time of most of the rest of the sky, though there is nothing particularly special about this region that warrants extra attention. While this is perfectly acceptable and it is unlikely we will find a strategy more efficient than δ-Bands, if we can find a tessellation method that spreads out this overlap over a wider area for a similar overhead cost then it might be preferable to a straight δ-Bands tiling. We will look at two ways of doing this, one

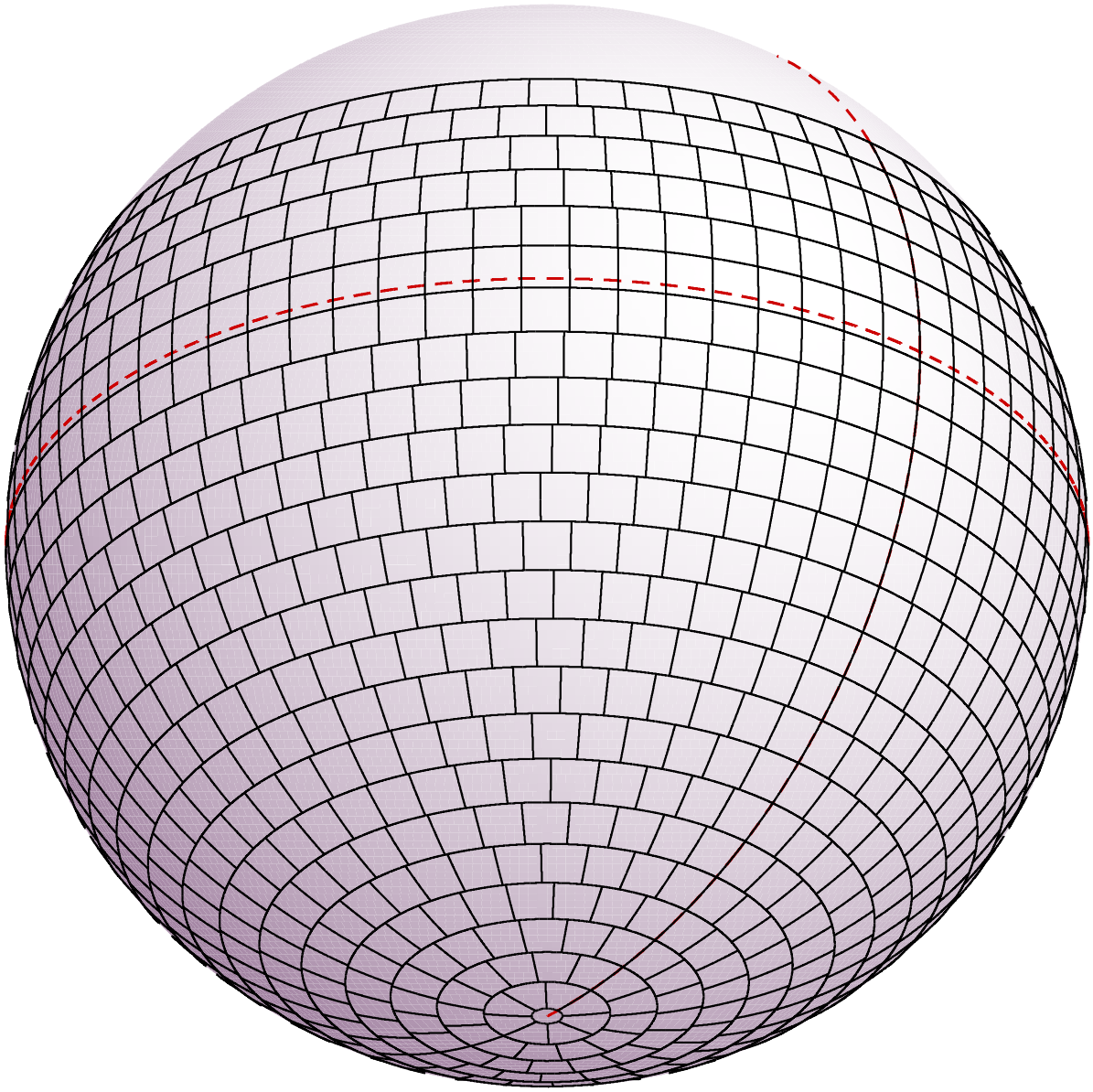

Fig. 3.— A view of the Declination Bands tessellation pattern projected onto a sphere. The black lines show the field boundaries for the tessellation pattern. The projection is orthographic and displayed as if viewed from outside the celestial sphere, and the projection centre is located at $\alpha = 43.55°$ $\delta = -29.61°$ (the centre of a field in band 12). North is up (the North Celestial Pole is off the top edge of the view, the SCP is towards the bottom of this view at the centre of the small circular field), east is to the left, with the equator and $\alpha = 0°$ marked with the red dashed lines.

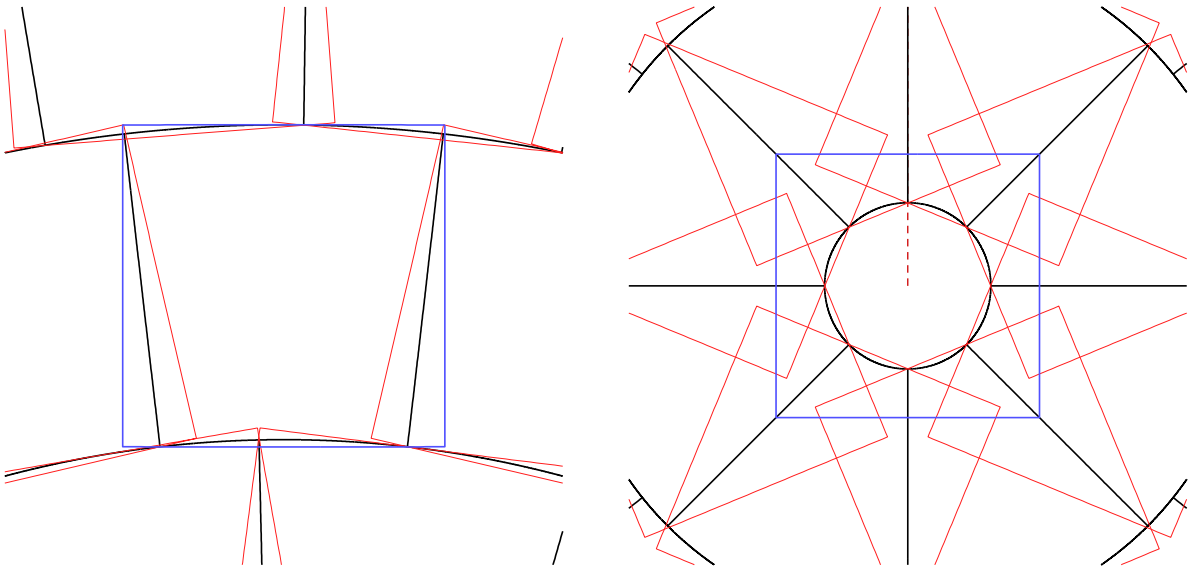

Fig. 4.— (Left panel) Close up of a δ-Bands field in band 20 to show field overlaps. Black lines show the tessellation pattern, the blue square shows the simplified approximation to the ASKAP FoV overlaid on the field in the centre of this view, while the red squares are the FoVs for the surrounding eight fields. North is up, east is to the left. (Right panel) The same but centred on the SCP field.

is a modification to this method in the polar region, the other is to use HEALPix instead which may result in similar amounts of overlap in all regions.

3.3. Modified Declination Bands

In order to reduce the concentration of overlapping fields towards the SCP region for the standard Declination Bands tessellation we have tested a method to spread the overlap over the entire South Pole cap region. For this modified Declination Bands tiling the standard method was used in the region from the northern boundary down to some chosen transition declination, $\delta_{transition}$, which is in the Southern Hemisphere and is the declination at the base of the last band of the standard δ-Bands method. South of $\delta_{transition}$ we use an alternative tessellation method to cover the South Polar Cap region, which in this case is essentially the δ-Bands method rotated 90°, and thus the equations needed are similar to those for the standard method.

In the alternative region we calculate the number of fields required to fill the region by using a coordinate system λ (longitude) and ϕ (latitude), centred on the SCP, and treating

it as if we were fitting a circular region at the equator. The first step was to determine the number of fields along a geodesic line going through the SCP (e.q. the $\alpha = 90°/270°$ line) between the points where it crosses $\delta_{transition}$, which is our 'equator' along $\phi = 0°$. If the number of fields is odd (which occurs in all cases we are looking at here) a band of fields is placed with their field centres along the $\phi = 0°$ out to where $\delta_{transition}$ is crossed. If the number of fields were even then two band would be calculated either side of the $\phi = 0°$ line. From these initial central bands further bands were calculated to fill the remainder of the polar cap region out to $\delta_{transition}$ (as the pattern is symmetric about $\phi = 0°$ only one half needed to be calculated, the other was simply mirrored). Fig. 5 shows one example of this configuration (see below).

Table 2 shows the results of replacing various numbers of standard bands with the alternative method. The first row of the table gives the results without an alternative region (as given in the previous sections), while the second only replaces the SCP field and so is no different from the standard method. The subsequent rows show the effect of replacing bands all the way up to the band just south of the celestial equator with the alternative tessellation.

The table shows that replacing the last four bands in the standard pattern has no effect on the number of fields required to cover the sky, essentially just resulting in a rearrangement of the positions of existing fields. If we replace the lower 5 to 12 bands with the alternative method we make a small saving in the number of fields, ranging from one to four less than the standard method. The most efficient combination is to replace the lowest six bands. Once $\delta_{transition}$ shifts to cover bands further north than $-30°$ the alternative method becomes less efficient than the standard method. If we continue until nearly the entire Southern Hemisphere is within the alternative region we would require up to ten more fields as the alternative method begins to suffer from the same issues close to the equator that we are trying to avoid at the SCP.

While useful, the motivation for using an alternative scheme in the polar region is not minor improvements in efficiency, with a few fields more or less making little difference for the survey. We need to know if the alternative method is effective at spreading out the overlap that is concentrated near the SCP in the standard method. Fig. 5 shows the region surrounding the SCP where we replace the last six bands with the alternative method (the most efficient combination). The boxes for the simplified ASKAP fields are plotted for the alternative region to show the overlap between fields, and at the transition between the two tessellation methods.

There is some small areas of overlap between neighbouring fields in the same band (the same as the wrap overlap in the standard region), but the main overlap regions in

Table 2. The effect on the number of fields and the efficiency of the Declination Bands technique of replacing fields around the South Celestial Pole with an alternative method of tessellation.

Bands Replaced	Replacement Rows	$\delta_{transition}$	Total Fields	Alternative Fields	Efficiency	Notes
		(°)			(%)	
(1)	(2)	(3)	(4)	(5)	(6)	
0	0	—	1201	0	95.34	No Alternative region
1	1	-88.36	1201	1	95.34	Pattern identical to standard method
2	3	-83.29	1201	9	95.34	
3	5	-78.26	1201	23	95.34	
4	7	-73.20	1201	43	95.34	
5	9	-68.12	1199	67	95.50	
6	11	-63.02	1197	97	95.66	Most efficient
7	13	-57.90	1200	137	95.42	
8	15	-52.77	1200	179	95.42	
9	17	-47.64	1199	225	95.50	
10	19	-42.49	1199	277	95.50	
11	21	-37.34	1199	333	95.50	
12	23	-32.18	1200	393	95.42	
13	25	-27.01	1202	457	95.26	
14	27	-21.84	1203	523	95.18	
15	29	-16.66	1202	589	95.26	
16	31	-11.48	1208	663	94.79	
17	33	-6.29	1209	733	94.71	
18	35	-1.10	1211	805	94.55	Replace entire Southern sky

Note. — Col. (1): The number of polar bands replaced by the alternative tessellation. Col. (2): The number of bands of the alternative method required to replace the polar fields. Col. (3): The transition declination between the standard δ-Bands tessellation region (to the north of $\delta_{transition}$) and the alternative method region (south of $\delta_{transition}$). Col. (4): The total number of field to cover the survey area (in both the standard and alternative regions). Col. (5): The number of fields covering the alternative method region only. Col. (6): Efficiency of the overall tessellation pattern (standard plus alternative) expressed as a percentage (target area of the survey divided by the area covered by all of the fields).

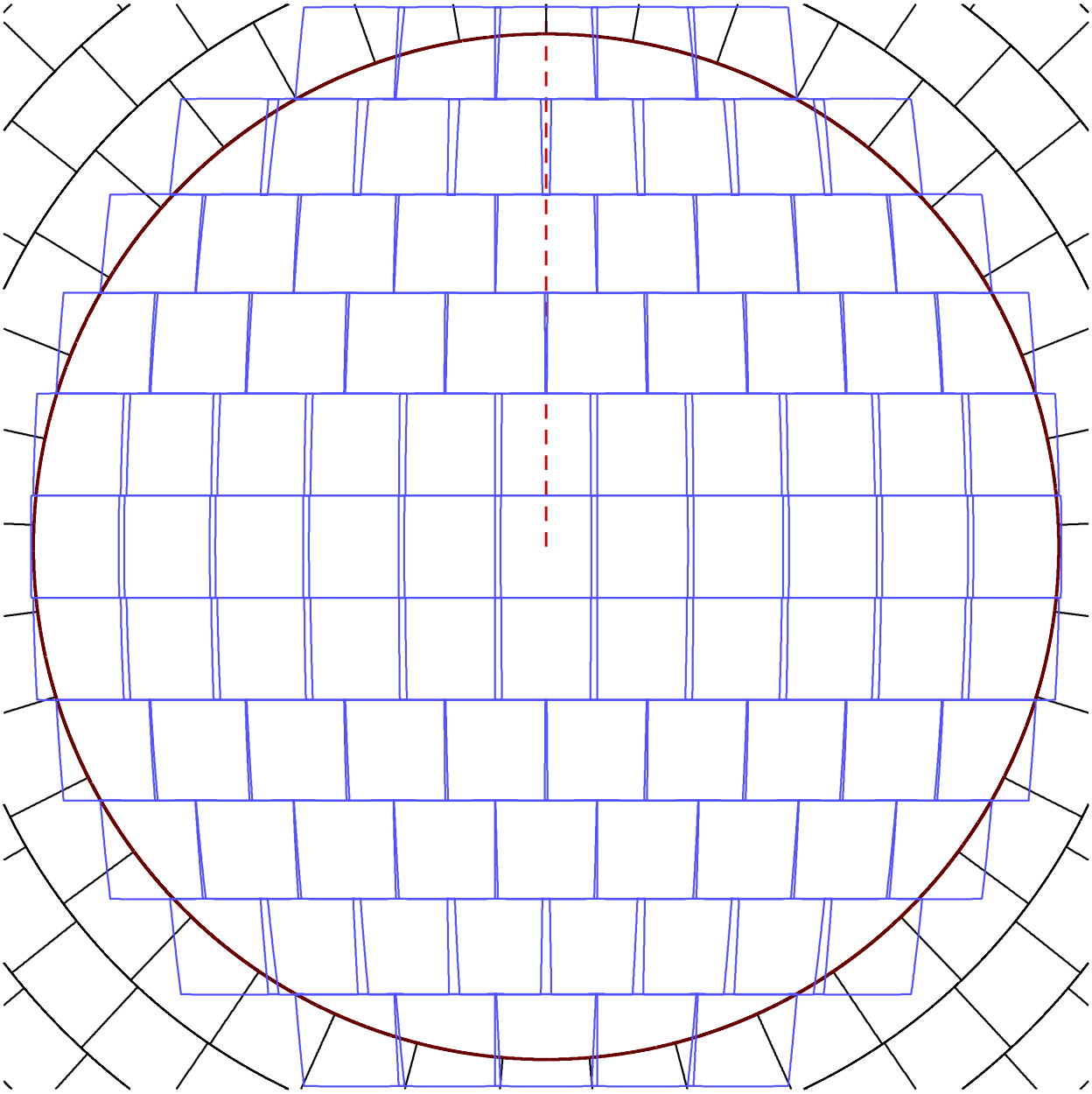

Fig. 5.— The field pattern for one configuration of the Modified Declination Bands tessellation in the SCP region, in this case replacing the last six bands of the standard Declination Bands tiling with the alternative method. The tessellation for the standard method region is show with the black lines, with the blue squares showing the positions of the fields for the alternative region. The thick dark red line marks the transition declination between the two methods, $\delta_{transition}$. The SCP is at the centre of the image, with the red dashed line marking the $\alpha = 0^{\circ}$ line. The projection is orthographic.

this configuration are the alternative fields that extend north of $\delta_{transition}$. A few fields are even centred north of $\delta_{transition}$. While this leads to reasonably large overlap areas in a ring around the sky above $\delta_{transition}$, the regions where more than two fields overlap are minimal compared to the standard tiling (see fig. 4, right panel). As we can change the position of $\delta_{transition}$ we can also move the location of this overlap ring if needed with little change to the survey efficiency. Additionally there may be some adjustment room between alternative bands to bring some overlap back south of $\delta_{transition}$ (though this may increase the number of fields required slightly).

The Modified Declination Bands tessellation has some small advantages over the standard tiling when it comes to the location of overlap regions, but otherwise will make little difference to the overall survey. Ultimately the survey team will need to decide if this small advantage is worth the complication of using two field positioning schemes. For the WNSHS, the proposed northern polar cap survey, the alternative scheme may be the more efficient method to use for the whole survey area, though this would have to be examined with fields approximating the new Westerbork focal plane array Apertif in the L-band.

4. HEALPix

Hierarchical Equal Area isoLatitude Pixelization (HEALPix, Górski et al. 2005) is a method of dividing up a sphere into approximately square equal area segments. It is most commonly used for large all-sky surveys at the later stages of data processing, when combining input data into full sky images that can be more easily handled. Most notably it has been used by recent Cosmic Microwave Background surveys such as the Wilkinson Microwave Anisotropy Probe, where all-sky analysis is important. It's main advantages for this are the hierarchical pixel indexing possible with this technique, the isolatitudinal pixel centres, and the constant area of all pixels across the sky. For our investigation we have explored whether HEALPix can also be used to calculate field positions for our all-sky survey without having overlap regions concentrated in one part of the sky like the δ-Bands tessellation.

4.1. Tessellation Pattern

The full details of the mathematics involved in defining the HEALPix tessellation pattern are described in Górski et al. (2005). Here we just give a brief description of the method we used to get a tiling pattern for field placement. The first step is the choice of a base-level division of a sphere into equal-area quadrilaterals (with curvilinear edges). The base

pixellation for HEALPix consists of three rows between the poles (one around each of the poles, the other around the equator), each of four approximately rhombus shaped pixels for a total of 12 base pixels. While equal area, the shape of the pixels varies with position on the sphere. The 12 pixel base that HEALPix uses is chosen so that the pixels are closest to being square (90° corners at the poles, minimised elongation of equatorial pixels), though equatorial pixels are elongated somewhat in right ascension, and polar pixels are generally elongated in Declination.

The base pixels are then divided further into a grid of equal area pixels to the desired resolution, controlled by the parameter N_{side} (a positive integer). This parameter defines the number of divisions along one side of the base pixel, so each base element contains a grid of N_{side}^2 pixels. Thus a total of $12N_{side}^2$ pixels of area $\Omega_{pix} = \pi/(3N_{side}^2)$ cover an entire sphere. The standard values of N_{side} are powers of two (at least as used in Górski et al. 2005), though the calculations are valid with other positive integers such as those we use in this work.

We require a HEALPix pixel size that fits within an ASKAP FoV (our $5.^\circ2 \times 5.^\circ2$ has an area of 27.021 sq. deg.), but is not so low that the efficiency of the method is significantly poorer than other methods. The lowest HEALPix resolution with a pixel area less than an ASKAP field is $N_{side} = 12$ ($\Omega_{pix} = 23.873$ sq. deg.), though whether individual fields fit the pixels depends on the shape variation of the pixels over the sky.

We will test HEALPix with this configuration to see if it is suitable for our field placement. We do not require the HEALPix software packages to perform these tests, just the equations defining the pixels/fields. The equations defining field centres for the ring pixel indexing scheme are set out in eqn. 2 to 9 of Górski et al. (2005), with different calculations in the polar caps and the equatorial bands. Pixel boundaries in both regions are defined by eqn. 19 to 22 of Górski et al. (2005). We can use these equations to get the field location, only using those fields that extend south of the northern boundary of the survey. The resulting field pattern has a 'fishing net' appearance, with the fields are all orientated at approximately 45° (see fig 6). Rows throughout the equatorial regions all have the same number of fields, $4N_{side}$ (fields at the equator are stretched in RA, and at higher latitudes they are stretched in Dec.), while each row south of $\delta = -\arcsin(2/3)$ ($= -41.^\circ81$, see Górski et al. 2005) has 4 fewer fields than the previous (the last row around the SCP having 4 fields).

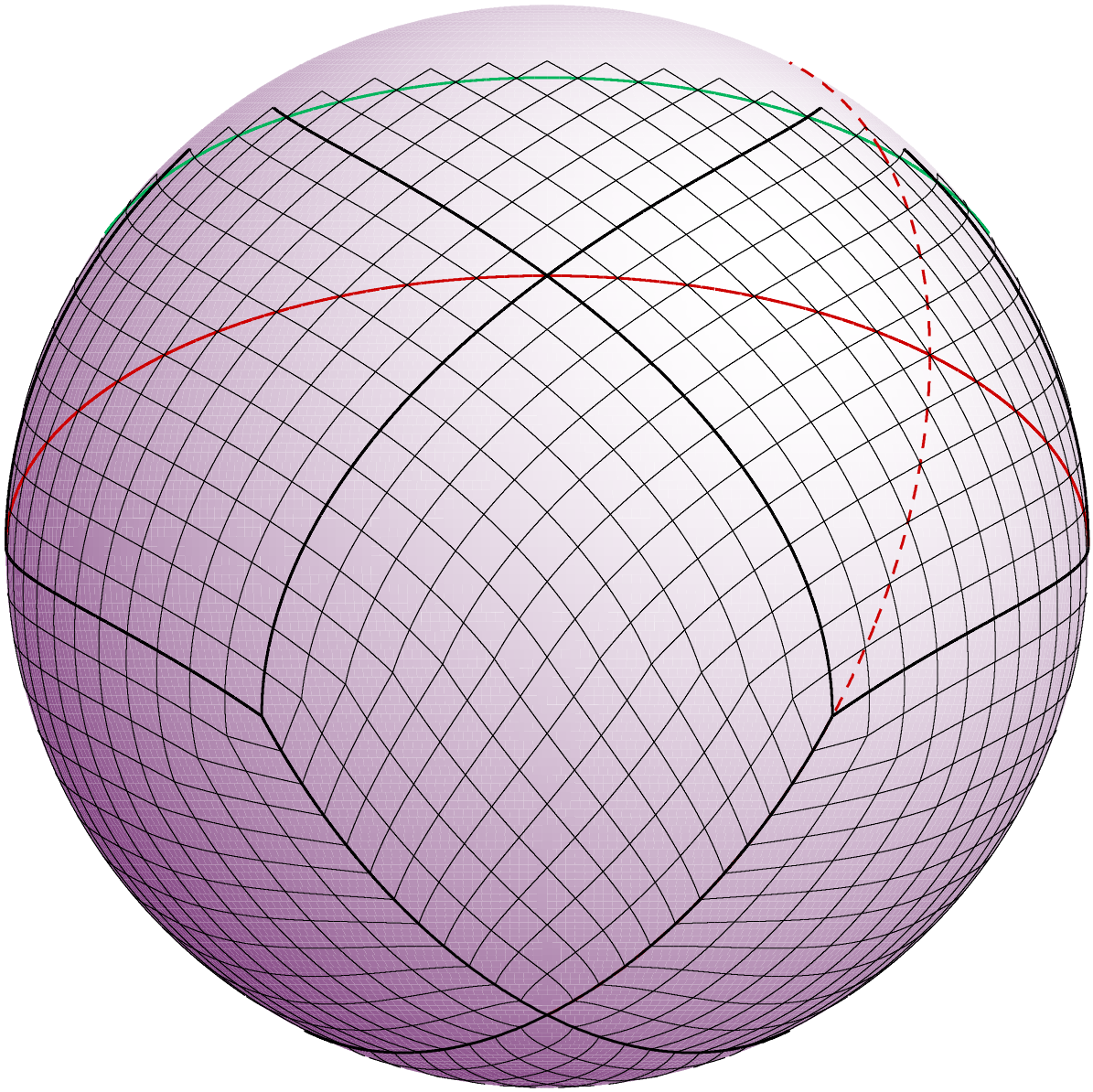

Fig. 6.— A view of the HEALPix tessellation pattern projected onto a sphere. The black lines show the field boundaries for the tessellation pattern, with the thicker lines showing the HEALPix base pixel pattern (cut off at the survey northern boundary). The projection is orthographic and displayed as if viewed from outside the celestial sphere, and the projection centre is located at $\alpha = 45°$ $\delta = -30°$ (the centre of a field in the 19th row from the northern limit of the survey). North is up (the North Celestial Pole is off the top edge of the view, the SCP is towards the bottom of this view at the centre of the small circular field), east is to the left, with the equator and $\alpha = 0°$ marked with the red dashed lines. The green dashed line marks the northern limit for WALLABY ($\delta = +30°$).

Table 3. Properties of each row calculated for the HEALPix tessellation pattern.

Row	δ_{centre} (°)	Fields	$\Delta\alpha_{centre}$ (°)	Efficiency (%)	Overlap (sq. deg.)	$\Delta\theta_{width}$ (°)	$\Delta\theta_{rows}$ (°)
(1)	(2)	(3)	(4)	(5)	(6)	(7)	(8)
1	+30.000000	48	7.500000	44.1746	724.072467	6.495191	7.361189
2	+26.387800	48	7.500000	88.3492	151.114671	6.718548	7.114620
3	+22.885380	48	7.500000	88.3492	151.114671	6.909635	6.916579
4	+19.471221	48	7.500000	88.3492	151.114671	7.071068	6.757760
5	+16.127620	48	7.500000	88.3492	151.114671	7.204840	6.631632
6	+12.839588	48	7.500000	88.3492	151.114671	7.312470	6.533552
7	+9.594068	48	7.500000	88.3492	151.114671	7.395100	6.460218
8	+6.379370	48	7.500000	88.3492	151.114671	7.453560	6.409330
9	+3.184739	48	7.500000	88.3492	151.114671	7.488417	6.379370
10	0.000000	48	7.500000	88.3492	151.114671	7.500000	6.369477
11	-3.184739	48	7.500000	88.3492	151.114671	7.488417	6.379370
12	-6.379370	48	7.500000	88.3492	151.114671	7.453560	6.409330
13	-9.594068	48	7.500000	88.3492	151.114671	7.395100	6.460218
14	-12.839588	48	7.500000	88.3492	151.114671	7.312470	6.533552
15	-16.127620	48	7.500000	88.3492	151.114671	7.204840	6.631632
16	-19.471221	48	7.500000	88.3492	151.114671	7.071068	6.757760
17	-22.885380	48	7.500000	88.3492	151.114671	6.909635	6.916579
18	-26.387800	48	7.500000	88.3492	151.114671	6.718548	7.114620
19	-30.000000	48	7.500000	88.3492	151.114671	6.495191	7.361189
20	-33.748989	48	7.500000	88.3492	151.114671	6.236096	7.669887
21	-37.669887	48	7.500000	88.3492	151.114671	5.936586	8.061326
22	-41.810315	48	7.500000	88.3492	151.114671	5.590170	8.376949
23	-46.046836	44	8.181818	88.3492	138.521782	5.678755	8.410724
24	-50.221039	40	9.000000	88.3492	125.928893	5.758448	8.294076
25	-54.340912	36	10.000000	88.3492	113.336004	5.829612	8.192623
26	-58.413662	32	11.250000	88.3492	100.743114	5.892557	8.104942
27	-62.445854	28	12.857143	88.3492	88.150225	5.947543	8.029874
28	-66.443536	24	15.000000	88.3492	75.557336	5.994789	7.966478
29	-70.412332	20	18.000000	88.3492	62.964446	6.034478	7.913993
30	-74.357529	16	22.500000	88.3492	50.371557	6.066758	7.871816
31	-78.284148	12	30.000000	88.3492	37.778668	6.091746	7.839474
32	-82.197003	8	45.000000	88.3492	25.185779	6.109533	7.816616
33	-86.100764	4	90.000000	88.3492	12.592889	6.120180	7.802997

Note. — Col. (1): Row number, starting from the Northern edge of the survey. Col. (2): Declination of the field centre for all fields in the row. Col. (3): Number of fields per row. Col. (4): The RA separation between the centre of fields in the same row. Col. (5): Efficiency of the fields within each row (area of the HEALPix pixels in the row, excluding areas outside the survey region, divided by the area of the fields covering that row). Col. (6): The overlap area between fields in a row or the area observed in excess of that required for the row (the area covered by the fields in that row minus the area of the HEALPix pixels in the row, excluding areas outside the survey region). Col. (7): The angular width of the HEALPix pixels in a row in the RA direction. Col. (8): The angular distance in the Dec. direction between the centres of the fields in the rows immediately north and south of the current row, approximating the height of the current row. For the final row this is the distance between the second last row and the SCP.

4.2. Results

Using a HEALPix $N_{side} = 12$ configuration, with the northern edge of the survey set to $\delta = +30°$, there are 1320 fields extending into the WALLABY target area. This is 119 more fields than δ-Bands, a significant extra investment of time (approximately 40 days extra time on-sky, plus overheads). The fields cover a total sky area of 35668.33 sq. deg., some 4728.61 sq. deg. over the the 3π steradians target area, and 3215.55 sq. deg. more than δ-Bands. HEALPix with $N_{side} = 12$ is 86.74% efficient, significantly lower than δ-Bands. This assumes we cover the entire WALLABY target area, but as we will see there is a significant issue with shape variation of fields over the sky.

Table 3 shows the details of the HEALPix tessellation pattern field positions. There are 33 interlocking rows in all, 9 in the Northern Hemisphere, one equatorial, and the remaining 23 in the Southern Hemisphere (a full $N_{side} = 12$ sphere would have the same number in the North, for a total of 47 rows). Unlike δ-Bands, the rows of HEALPix pixels are only contiguous at the corners of the fields due to the $\sim 45°$ rotation of the fields, with fields from the rows above and below meeting at the same points (except for some locations in the polar region). In general HEALPix has more rows with less fields than δ-Bands. The top HEALPix row is centred exactly on the northern boundary of the survey, so half of each field in that row is outside the target area, halving the efficiency of that row.

The other 32 rows have identical efficiency as we calculate it (not taking into account any area missed by the tessellation). This is because the target area of each row is just the number of fields times the area of a HEALPix pixel, while the area covered is the number of fields by the ASKAP field area. So the efficiency in this case reduces to the HEALPix pixel area divided by the ASKAP field area for all rows within the survey target area, which is the same at all locations. Likewise, the apparent overlap between fields amounts to the same area, 3.1482 sq. deg., for all fields everywhere except at the northern boundary. So the total overlap is just the number of fields times this overlap area, plus the area north of survey boundary.

All rows centred at $\delta \geq -41.^{\circ}81$ ($= -arcsin(2/3)$) contain 48 fields with the same RA separations, $7.^{\circ}5$ (or 0.5 hours), with shape variations accounting for the differences in angular separation along those rows. Fields along the equator are stretched horizontally, with fields at higher latitudes stretched vertically. Fig 7 illustrates this stretching of HEALPix fields both vertically (magenta) and horizontally (green) with position on the sky (the last two columns of table 3). The horizontal line at $7.^{\circ}3539$ is the diagonal width/height of our square approximation to the ASKAP field, so if the separation between fields is larger than this there will be a gap between fields.

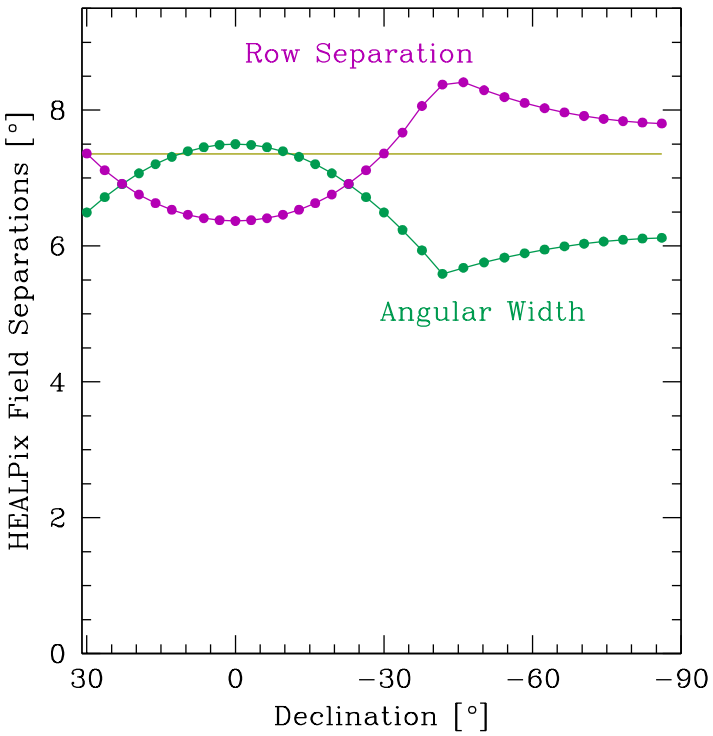

Fig. 7.— Plot indicating the relative separation between HEALPix fields as a function of Declination. The green line shows the angular width of the HEALPix pixels in a row in the RA direction, the angular separation between the centres of fields in the same row. The magenta line shows the angular separation in the Dec. direction between the centres of the fields in the rows immediately north and south of the current row, approximating the height of the current row (for the final row this is the distance between the second last row and the SCP). The horizontal line at $7\overset{\circ}{.}3539$ is the diagonal width/height of our square approximation to the ASKAP field (i.e. the maximum separation without leaving a gap).

The fields at around $\delta = \pm 22\overset{\circ}{.}89$ (rows 3 and 17) are the closest to being square, and this is one of the few regions of the sky where the HEALPix pixels fit entirely within our simplified ASKAP field model. Towards the equator the separation between fields in the same row exceeds the diagonal width of the model ASKAP field, so there is no overlap between fields in these rows. However, the vertical separation between rows in this region allows the rows immediately to the north and south to overlap in these regions, filling in the gaps. Looking to the immediate South of the declinations where the fields are approximately square, where fields are stretched vertically, we see the opposite situation, with fields to the east and west compensating for gaps between fields to the north and south. This holds throughout the equatorial regions where there are an equal number of fields per row. Fig. 8

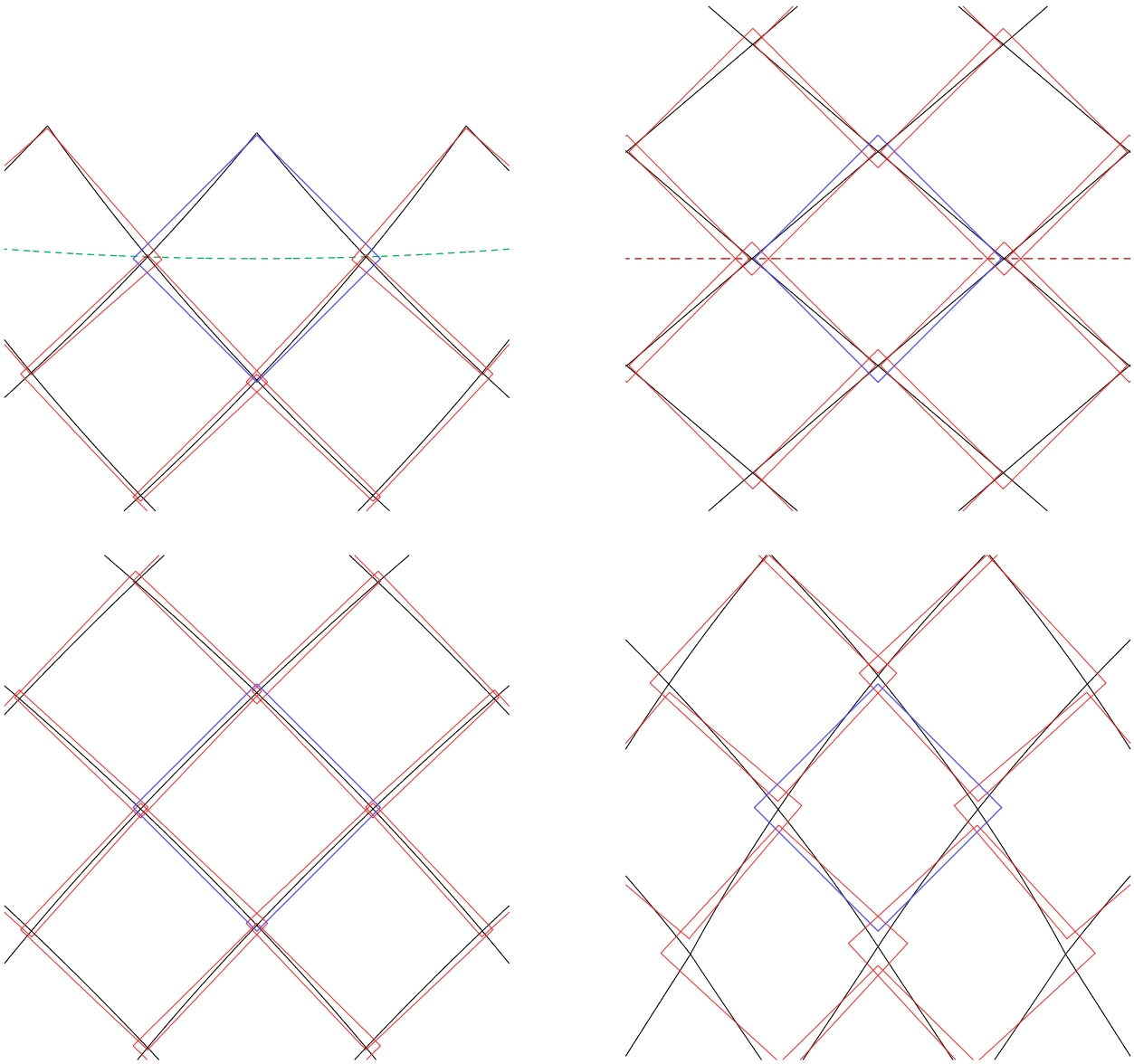

Fig. 8.— Close up of four *equatorial* fields and their surrounds in the HEALPix tessellation pattern. Black lines show the tessellation pattern, the blue squares shows the simplified approximation to the ASKAP FoV overlaid on the field in the centre of this view, while the red squares are the FoVs for the surrounding fields (up to eight depending on the location). North is up, east is to the left. The four panels show fields at the following locations: Top left - the northern boundary (row 1 centred at $\delta = +30°$); Top right - the celestial equator (row 10 centred at $\delta = 0°$); Bottom left - a field at $\delta = -22.^{\circ}89$, where the fields are approximately square (row 17); Bottom right - a field at $\delta = -37.^{\circ}67$, the row prior to the change in how HEALPix calculates pixel dimensions (row 21).

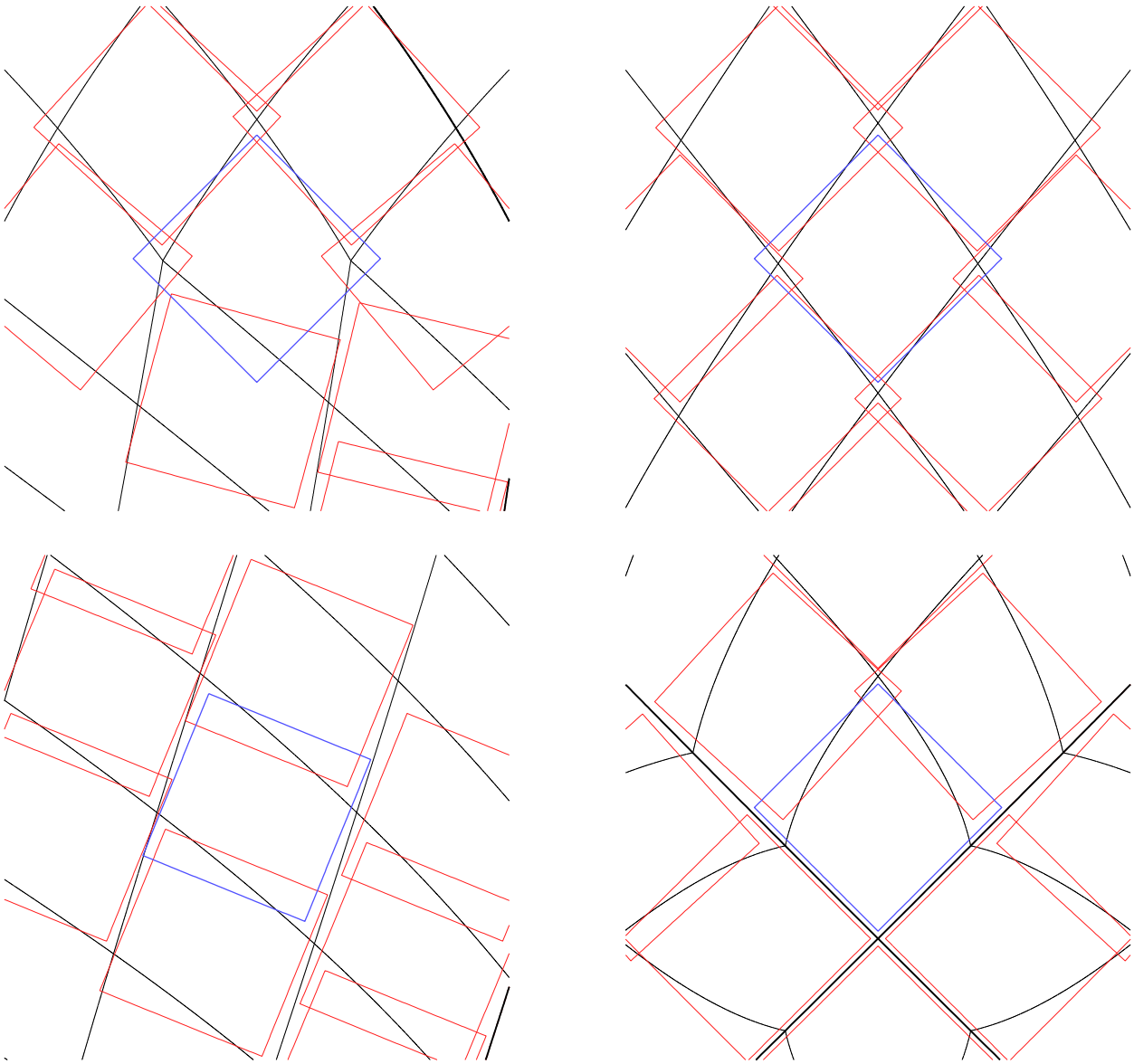

Fig. 9.— Close up of four *polar cap* fields and their surrounds in the HEALPix tessellation pattern, showing where the HEALPix tessellation breaks down. Black lines show the tessellation pattern, the blue squares shows the simplified approximation to the ASKAP FoV overlaid on the field in the centre of this view, while the red squares are the FoVs for the surrounding fields (up to eight depending on the location). North is up, east is to the left. The four panels show fields at the following locations: Top left - the row where the transition from equatorial to polar cap calculation occurs (row 22, field 2, centred at $\delta = -41.^{\circ}81$); Top right - a field in row 27 sitting along the centre line of a base pixel (row 27, field 4, centred at $\alpha = 45^{\circ}, \delta = -62.^{\circ}45$); Bottom left - another field in row 27, but closer to a base pixel edge (row 27, field 2, centred at $\alpha = 19.^{\circ}29, \delta = -62.^{\circ}45$); Bottom right - one of the four polar fields (row 33, $\delta = -86.^{\circ}10$).

shows four examples of fields in the equatorial region (northern boundary, equator, the square fields in row 17, and the last full equatorial row), all of which show overlap with neighbouring fields that fills in any gaps caused by shape distortion. However, this breaks down in the polar cap region where each subsequent row has less pixels.

At $\delta \geq -41.^{\circ}81$ ($= -arcsin(2/3)$) there is a transition in the HEALPix pixel calculations, and each row south of this has four less fields than the previous. The result is that the gaps between fields do not get covered by surrounding fields as they do in the equatorial region. Additionally there is greater shape variations in the polar cap region than is seen in he equatorial regions, with shapes varying within rows as well as between them (in the equatorial region all fields in a row are the same shape). Fig 9 shows four fields in the polar cap region that illustrate several gaps between fields caused by shape variations in the HEALPix tessellation. The first panel (top left) shows one of the more extreme cases, the row where the transition from equatorial to polar calculations occurs. Some fields in this row are highly distorted due to this transition, leaving large gaps between fields if they follow the HEALPix positions. The top right and bottom left panel both show different nearby fields in row 27 (they share one of the red surrounding fields, the one right of centre and left of centre, respectively). While the fields in the first of these two panels cover the region relatively well, there are neighbouring fields in the second panel that do not overlap at any point. The final panel (bottom right) shows the SCP region, where fields centred at the HEALPix positions leave thin gaps between the polar fields, such that the SCP itself (lower centre of this panel where the thick black lines cross) is outside the fields.

While HEALPix does do the task we originally investigated it for, spreading overlap over the whole sky instead of concentrating it in one region, it otherwise performs very poorly compared to δ-Bands. It is a far less efficient tessellation method, requiring more than a month extra observing time. But the real drawback of this method is its inability to cover the entire sky without gaps between fields. While it is conceivably possible to make adjustments to the field positions to cover these gaps, doing so would remove some of the other advantages of the method and potentially create issues in other parts of the sky. The only other alternative would be to use a smaller pixel area by setting $N_{side} = 13$. This would cover the gaps, but would be even less efficient than $N_{side} = 12$ and adding months to the survey observing time. It is unlikely this method will be useful for generating our fields placements, but it will be useful after observations have taken place for all-sky data products.

5. Survey Implications

It is clear from this investigation that of the two methods explored Declination Bands is a better technique for calculating field placements for WALLABY. It is significantly more efficient than HEALPix, allows some flexibility in field positioning, and most importantly does not leave any gaps between neighbouring fields like HEALPix does. Though the exact field parameters are yet to be finalised at the time of this memo, it should be possible to adapt Declination Bands to suit most of the proposed field configurations. The modified δ-Bands tessellation method for the SCP region may be a useful variation on the standard technique, but whether its small advantages make it worth implementing needs to be determined by the team. The final field positions, and the number of fields required, should not be determined until the parameters of the ASKAP field are well understood.

The next stage of this process would be to test the sensitivity coverage over the sky for δ-Bands using a more realistic model of the ASKAP field, generated from the current best models of the beam positions and proposed dithering patterns. This is particularly important for understanding the overlap we need to account for between field, and will be the subject of the next memo in this series.

REFERENCES

Barnes, D. G., et al. 2001, MNRAS, 322, 486

Górski, K. M., Hivon, E., Banday, A. J., Wandelt, B. D., Hansen, F. K., Reinecke, M., & Bartelmann, M. 2005, ApJ, 622, 759

Skrutskie, M. F., et al. 2006, AJ, 131, 1163

Staveley-Smith, L. 1997, PASA, 14, 111